RESONANT AND LOCALIZED BREATHING MODES IN TERMINAL REGIONS OF THE DNA DOUBLE HELIX

B. F. PUTNAM, L. L. VAN ZANDT, E. W. PROHOFSKY AND W. N. MEI, *Department of Physics, Purdue University, West Lafayette, Indiana* 47907

ABSTRACT A Green's function approach is used in constructing a dynamic model of a semi-infinite length of the DNA homopolymer B poly(d$\mathcal{G}$) · poly(d$\mathcal{C}$). Considerable attention is focused on the hydrogen bond stretching close to the terminus. A melting (or breathing) coordinate (M) is defined as an average over the three linking hydrogen bond stretches in a unit cell. The thermal mean squared amplitude of (M) is enhanced at the chain end compared with the interior. Spectral branches at 69, 80, and 105 cm^{-1}, as well as a local mode at 75 cm^{-1}, are primary contributors to the enhancement. We suggest that this fact can affect the thermal melting of a DNA double helical homopolymer, enhancing the tendency to start from an end (if one is available). We show how certain infinite chain modes with small (M) amplitude can turn into breathing modes near the terminus, and suggest that the same phenomenon may occur near other specific base-pair sequences. There is also considerable attention paid to the low microwave region from ~0 to 1.75 cm^{-1}. The thermally activated modes in this frequency region contribute ~$(0.02\ Å)^2$ to $\langle M^2(0)\rangle$ at 400 K, approximately two orders of magnitude greater than for $\langle M^2(\infty)\rangle$. Most important however, is the existence of narrow resonant modes in this frequency region. Particularly pronounced resonances near 0.03 cm^{-1} and 0.08 cm^{-1} (~0.9 and 2.4 GHz) amplify $M^2(0)$ at the terminus by about four orders of magnitude over the infinite chain value $M^2(\infty)$.

INTRODUCTION

We are concerned with the dynamic properties of DNA and RNA polymers of various conformations and base-pair sequences (1, 2). Up to this time, much of the work has been on DNA (or RNA) homopolymers or copolymers with helical symmetry, as discussed by Higgs (3). This symmetry permits the secular equation to be factored so that the normal modes are easily calculated.

In the present paper, the presence of a terminus (or free end) is treated as a defect on the long helical DNA poly(d$\mathcal{G}$) · poly(d$\mathcal{C}$). This cut chain perturbation consists of setting to zero those internal force constants describing the interaction between any atom of the double helix with any other atom on the other side of an imaginary plane dividing unit cells (0) and (−1), see Fig. 1. This approach of cutting an infinite helix to produce a semi-infinite chain with a terminus is the simplest approach to the problem that contains the effects of the large number of interactions of the semi-infinite chain and is still a finite mathematical problem. This comes about because of the unique feature of a Green's function analysis. This was pointed out long ago by Lifshitz and Pekar (4).

Ising model calculations (5, 6) that take into account complications such as the free ends have been performed previously on DNA polymers. These models are purely statistical and do not directly consider the detailed internal structure of each unit cell, which is viewed as a point entity with an associated binding energy.

In this paper we report the results of a detailed and exact (within the harmonic approximation) treatment of the effect of a terminus on the hydrogen bond stretching of the DNA double helix. We consider a semi-infinite strand of DNA rather than a finite section with two free ends. This involves the assumption that the two ends are far enough apart that they do not interact. This approximation has been shown to be adequate since we have found the effects of the terminus to be unimportant (even at resonances) at distances greater than about 10 base-pair units. As expected, for frequencies lying within the dispersion branches of the infinite (perfect) helix, the perturbed modes are still wavelike.

Considerable effort has gone into the study of the melting, or strand separation of the double helix. The dissociation of hydrogen bonds in this process should be a strong function of the separation of the heavy end atoms of the hydrogen bond. A "melting" coordinate (M) is defined (2) as the average hydrogen bond stretching in a unit cell. In a complicated macromolecule many factors such as a free end or local sequence can give rise to unusual thermal amplitudes of this hydrogen bond M value. Because of the importance of this particular property we have chosen in this paper to pay particular attention to these amplitudes. In principle one solves for all the amplitudes of all the degrees of freedom at a free end, but one must specifically accumulate all of these data. We have simplified our data output by selectively scanning these hydrogen bond "breathing mode" amplitudes for display.

Because of this same bias toward concentrating on the hydrogen bond breathing modes we have been able to concentrate our effort on certain frequency ranges rather than scanning the entire frequency spectrum. In previous calculations on infinitely long double helical polymers we have found that many vibrational bands can be characterized as predominantly breathing modes of the hydrogen bond heavy-atom displacements. We have referred to such bands as "melting modes" (2, 7). Because of the structure of the Green's function one expects that large melting modes near the terminus would be close in frequency to melting modes of the uncut infinite helix. One even talks about oscillator strength or spectral density of the localized mode as being taken from the unperturbed modes. We have therefore selectively scanned frequency regions near the frequencies of unperturbed infinite helix melting modes.

We have discovered the existence of resonant breathing modes, with strong resonant behavior in the $M^2(0)$ coordinate which is adjacent to the terminus. Three of these occur in the low microwave region at ~0.03, 0.083 and 0.087 cm^{-1} (~0.9 and 2.5 GHz). The existence of these "free end" resonant melting modes could have profound implications regarding the living cell's response to radiation at the resonant microwave frequency. Resonant microwave effects, as opposed to simple thermal effects, have been reported (8). Some work in microwave absorption by double helical poly(d$\mathcal{G}$) · poly(d$\mathcal{C}$) has been done (9). Microwave absorption in DNA samples has been observed (10).

We also look at the behavior of the hydrogen bond stretching within the infinite chain breathing mode branches near 69, 80, and 105 cm^{-1}, and within the five adjacent gap regions. A localized breathing mode for each of the two semi-infinite strands is found within two of these gaps. Graphs are displayed from which the thermal mean-square displacement $\langle M^2 \rangle$ may be deduced. We calculate that $\langle M^2(0) \rangle$ adjacent to the cut is about a factor of two greater than $\langle M^2(\infty) \rangle$ far from the cut. We suggest that the hydrogen bonds in the vicinity of the terminus are somewhat less stable and that this can alter the melting behavior.

FORMALISM FOR THE TERMINATED HELIX

We are concerned here with the solutions of the eigenvalue equation

$$(F - \omega^2 + C)q = 0. \tag{1}$$

This equation describes an infinite strand of the DNA double helical homopolymer B poly(d$\mathcal{G}$)·poly(d$\mathcal{C}$) which has been severed between the unit cells (−1) and (0). The perturbing force constant matrix (C) is defined as the change in the force constant matrix (F) of the perfect helix necessary to bring about this separation. The perturbation breaks the helical symmetry thereby making the description of the normal modes much more difficult. However, since C is a matrix of relatively low dimensionality, Eq. 1 may be conveniently solved in terms of the Green's function (g) of the perfect helix.

The Green function for the perfect helix may be written (11) in terms of the solutions of the perfect helix eigenvalue equation, that is,

$$g_{\alpha\alpha'}(\ell, \ell'; \omega^2) = (\omega^2 - F)^{-1} = \frac{1}{\pi} \sum_j \int_0^\pi \frac{\mathrm{Re}[q_\alpha^j(\theta)\, q_{\alpha'}^{j*}(\theta)\, e^{i\theta(\ell - \ell')}]}{\omega^2 - \omega_j^2(\theta)}\, \mathrm{d}\theta. \tag{2}$$

α refers to an atomic coordinate in the unit cell ℓ. The label j is the branch index for the point θ in the one-dimensional Brillouin zone.

If ω^2 lies within a branch gap of the perfect helix dispersion curves, then the integrand in Eq. 2 is nonsingular and g may be easily evaluated. Premultiplying Eq. 1 by g yields

$$(1 - gC)q = 0.$$

The condition for a localized (gap) mode is $D(\omega^2) = \det(1 - gC) = 0$.

If ω^2 lies within one or more phonon dispersion branches of the perfect helix, then Eq. 2 involves an integration over one or more singularities. We may handle this by a mathematical trick which also has a physical interpretation (12). Give ω^2 a small imaginary part $i\gamma$ and take the limit as $\gamma \to 0$. An imaginary contribution to ω^2 corresponds to a finite relaxation time which goes to infinity as $\gamma \to 0$ (12). The proper evaluation of the Green function is discussed in Appendix A.

The Green function for the severed helix G may similarly be expressed in terms of the perturbed normal modes $q(\omega)$, that is,

$$G_{ij}(\omega^2) = \lim_{\gamma \to 0} \int \frac{q_i(\omega')\, q_j^*(\omega')\, \rho(\omega')}{\omega^2 - \omega'^2 + i\gamma}\, \mathrm{d}\omega'. \tag{3}$$

The perturbed q are of course not known *a priori*, however G may be expressed and calculated in terms of known quantities.

$$G = (\omega^2 - F - C)^{-1} = (1 - gC)^{-1} g$$

which may be written (12, 13) as

$$G = g + gTg$$

where

$$T = C(1 - gC)^{-1}.$$

Using the identity (12, 13) employed in Appendix A,

$$\lim_{\gamma \to 0} \frac{1}{x + i\gamma} = P\left(\frac{1}{x}\right) - i\pi\delta(x),$$

we see, with reference to Eq. 3, that the imaginary parts of the diagonal elements of G are proportional to the perturbed squared amplitudes of vibration weighted by the perturbed densities of state. A thermal mean-square displacement amplitude may be obtained from (11–13)

$$\langle q_i^2 \rangle = \frac{2\hbar}{\pi} \int \frac{\mathrm{Im}[G_{ii}(\omega^2)]}{e^{\hbar\omega/kT} - 1} \mathrm{d}\omega.$$

The condition for a resonant (11–13) frequency ω_s^2 is

$$\mathrm{Re}[D(\omega_s^2)] = 0$$

where

$$D(\omega^2) = \det(1 - gC) = D_r + iD_i.$$

The half-width of the resonance (13) is

$$\Gamma = \frac{2D_i(\omega_s^2)}{[\mathrm{d}D_r(\omega_s^2)]/\mathrm{d}\omega}.$$

The above results may easily be extended to include a formalism for scattering. Eq. 1 may be rewritten (13) as

$$q = q_0 + gTq_0$$

where the incoming wave q_0 is a solution for the infinite helix. The singularities in g may be handled in such a way that at large distances from the cut, the reflected waves gTq_0 are travelling away from the cut (14). That is, $\omega^2 \rightarrow \omega^2 \pm i\epsilon$ where $[\mathrm{d}\omega^2(\theta)]/\mathrm{d}\theta$ is $(\pm)$. An alternative is to let $\omega^2 \rightarrow \omega^2 + i\gamma$ where γ corresponds to a finite relaxation time.

All of the above formalism may be couched in internal coordinates thereby making many of the following calculations easier to perform than in Cartesian coordinates. The use of internal coordinates is discussed in Appendix B. The method by which internal coordinates are used in reducing the dimensionality of the chain-severing perturbation is discussed in detail in Appendix C.

RESULTS AND DISCUSSION

In the following discussion we will be referring to graphs of $n(\omega)\mathrm{Im}G(\omega)$ vs. frequency ω. G is the severed helix Green function while $n(\omega)$ is the thermal occupation number at $T = 300$ K. The part of the Green function displayed belongs to the semi-infinite strand above the dashed line in Fig. 1 extending from units 0 to ∞. For this strand, as we move along the 3′ to 5′ direction on the guanine (cytosine) strand we are travelling away from (toward) the severed end. We expect that the essential results of this calculation are qualitatively similar but not identical for both semi-infinite strands.

There are three linking hydrogen bonds in each unit cell of the poly(d$\mathcal{G}$)·poly(d$\mathcal{C}$) double helix, see Fig. 1. A breathing or melting coordinate M is defined as an average over the three hydrogen bond displacements in a unit cell. Henceforth the average breathing in the unit cell n units from the cut will be denoted M $(n - 1)$. $M(\infty)$ refers to the infinite chain breathing "far" from the cut. The imaginary part of the diagonal elements of the severed helix Green function, $\mathrm{Im}(G)$, are calculated for the melting coordinate at various distances from the cut end. $\mathrm{Im}(G)$ is proportional to (ρM^2) where ρ is the perturbed density of states and (M^2) is the squared amplitude of the perturbed normal mode coordinate M. $\mathrm{Im}[G(\infty)]$ is essentially the imaginary part of the perfect helix Green function.

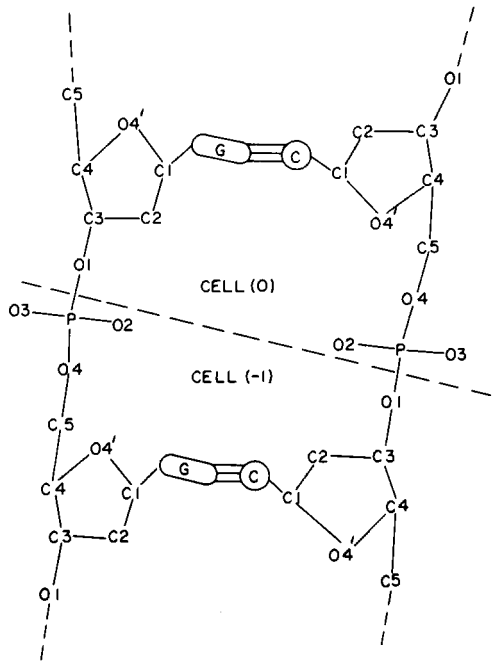

FIGURE 1 Portion of two unit cells of poly(d$\mathcal{G}$)·poly(d$\mathcal{C}$). The dashed line indicates the position of the cut. The P—O bonds cut are those cleaved by the restriction endonuclease enzymes.

First we make some general observations regarding the "in band" perturbed modes. The effect of the free end on the M coordinate is gone by the sixth unit cell from the end, i.e., $G(5) \approx G(\infty)$. Exceptions to this are the low microwave resonant breathing modes which are perceptible as far as 10 units from the cut.

As discussed in Appendix A, because of the one-dimensional nature of the DNA Brillouin zone, a finite relaxation time must be assumed in the immediate vicinity of the band edges. This was done for selected zone edge frequencies and it was found that for a realistic relaxation time of say, $\omega\tau = 20$, the displacements at the band edges do not significantly contribute to the thermal mean-square displacement $\langle M^2 \rangle$.

The infinite chain breathing mode dispersion branch extending from ~69.38 cm^{-1} at $\theta = 0$ to ~68.52 cm^{-1} at $\theta = \pi$, has a peak at ~70.38 cm^{-1} (7). See Fig. 2 *D*. Thus Im(G) is continuous from 68.52 to 69.38 cm^{-1} and from 69.38 to 70.38 cm^{-1}. In Fig. 3 we have plotted the imaginary part (weighted by the phonon thermal occupation number) of $G(0)$ and $G(\infty)$ for frequencies 68.7 to 69.375 cm^{-1}. A thermal mean-square displacement amplitude for the melting coordinate may be obtained from

$$\langle M^2 \rangle = \frac{2\hbar}{\pi} \int \frac{[\mathrm{Im}G(\omega^2)]\mathrm{d}\omega}{e^{\hbar\omega/kT} - 1}. \tag{4}$$

We have plotted the appropriately normalized integrand vs. ω. The normalization for this and the following similar graphs is chosen so that the mean-square displacement of the melting coordinate in $Å^2$, at 300 K, is equal to the area under the appropriate curve.

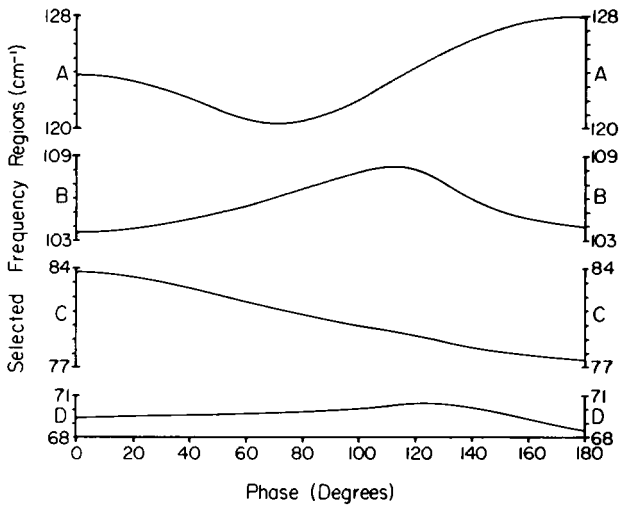

FIGURE 2 Selected phonon dispersion branches for the perfect infinite helix B poly(d$\mathcal{G}$)·poly(d$\mathcal{C}$). The abscissa is the phase difference between adjacent unit cells. *A* is a rocking mode branch while *B*, *C*, and *D* are breathing mode branches. These curves are from the work reported in reference 7.

Throughout this region of the branch, the coordinate $M(0)$ is amplified with respect to the infinite chain value $M(\infty)$. No resonance modes occur in this region. At the poly(d$\mathcal{G}$)·poly(d$\mathcal{C}$) melting temperature 400 K, $G(0)$ and $G(\infty)$ contribute $(0.014\ \text{Å})^2$ and $(0.009\ \text{Å})^2$, respectively to the integral, Eq. 4.

The Green functions for the part of this same branch from 69.4 to 70.35 cm^{-1} have been calculated and integrated over the frequency region. Again, no resonances occur in this region. Here, $M(0)$ is suppressed relative to $M(\infty)$. At 400 K, $G(0)$ and $G(\infty)$ contribute $(0.011\ \text{Å})^2$ and $(0.039\ \text{Å})^2$, respectively to the integral, Eq. 4.

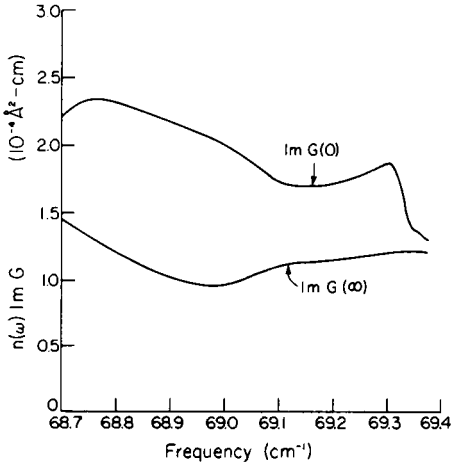

FIGURE 3 Imaginary parts of $G(0)$ [$\sim\rho M^2(0)$ adjacent to the cut] and $G(\infty)$ [$\sim\rho M^2(\infty)$ far from the cut] vs. frequency for a breathing branch region 68.7 to 69.375 cm^{-1}. $G(\infty)$ is essentially the perfect helix Green's function. G is weighted by the thermal occupation number $n(\omega)$, at T = 300 K, in this and the following similar graphs.

The largest breathing motion for poly(dG)·poly(dC) occurs in the branch extending from 77.58 cm^{-1} at $\theta = \pi$ to 83.72 cm^{-1} at the zone center, $\theta = 0$ (7). See Fig. 2 *C*. The largest infinite-chain breathing occurs, as expected, near the zone edge at ~83.7 cm^{-1}. From ~78 to ~81 cm^{-1}, Im[$G(0)$] is slightly suppressed relative to Im[$G(\infty)$], yet they both behave similarly as functions of frequency. Above ~81 cm^{-1}, as the infinite chain breathing becomes stronger, the breathing adjacent to the cut becomes suppressed. This behavior suggests that the hydrogen bonds at the terminus no longer breath at the infinite chain frequencies, and that probably a localized breathing mode exists in a nearby branch gap. Indeed, as will be discussed later, a localized breathing mode does appear in the branch gap immediately below this infinite chain breathing branch, contributing (0.1 Å)^2 to $\langle M^2(0)\rangle$ at 400 K. The $G(0)$ and $G(\infty)$ functions contribute (0.043 Å)^2 and (0.061 Å)^2 to $\langle M^2(0)\rangle$ and $\langle M^2(\infty)\rangle$, respectively, at 400 K. No resonance mode occurs in this branch.

The final and highest frequency breathing mode branch extends from 103.55 cm^{-1} at the zone center ($\theta = 0$) to 104.03 cm^{-1} at the zone edge ($\theta = \pi$), and has a peak at 108.26 cm^{-1} (7). Thus Im(G) is continuous from 103.55 to 104.03 cm^{-1} and from 104.03 to 108.26 cm^{-1}. See Fig. 2 *B*. For the first of these regions, Im$G(0)$ is suppressed relative to Im$G(\infty)$. In this frequency region, $G(0)$ and $G(\infty)$ contribute (0.012 Å)^2 and (0.016 Å)^2 to $\langle M^2(0)\rangle$ and $\langle M^2(\infty)\rangle$, respectively, at 400 K.

The Green functions for the remainder of this branch from 104.1 to 108 cm^{-1} have also been calculated. At the band edges where Im[$G(\infty)$] becomes large, Im[$G(0)$] is suppressed. From 104.5 to 106.25 cm^{-1} $G(0)$ is slightly amplified with respect to $G(\infty)$ while 106.25 to 107.5 cm^{-1}, $G(0)$ is slightly suppressed. The net effect is that both Green functions contribute ~(0.035 Å)^2 to $\langle M^2(0)\rangle$ and $\langle M^2(\infty)\rangle$ at 400 K. Again, there are no resonance modes in this branch.

There are five band gaps adjacent to these three breathing mode branches (7). The branch near 80 cm^{-1} shares an adjacent gap with the branch near 69 cm^{-1}. Localized modes are found by searching for zeroes of det($1 - gC$), as described previously and in Appendix B. The localized modes were normalized by setting $\frac{1}{2}\omega^2 \Sigma_i q_i^2 = \hbar\omega/(e^{\hbar\omega/kT} - 1)$. Since $q_i = \Sigma_{tt'} g_{it} C_{tt'} S_{t'}$, this condition becomes

$$\frac{1}{2}\omega^2 \sum_i \sum_{\substack{t,t' \\ t'',t'''}} S_t C_{tt'} g_{it'} g_{it''} C_{t''t'''} S_{t'''} = \frac{\hbar\omega}{e^{\hbar\omega/kT} - 1}.$$

The sums on the t are finite since $C_{tt'}$ is finite. The infinite sum on i may be performed using the orthonormality of the unperturbed vectors. Accurate values for the positions of the localized modes were obtained using the modified *regula falsi* method (15). The internal coordinate Green function was used. In order to ensure that no spurious solutions were introduced in the transformation to internal coordinates, we constructed the Green function in Cartesian coordinates and used only one internal coordinate, a generalized compression. The effect of this one internal coordinate is quite small in this frequency region of interest. Using the Cartesian ($1 - gC$) we evaluated det($1 - gC$) on either side of the previously found modes to ensure that det($1 - gC$) did indeed change sign. We assume that the internal coordinate mode is not spurious. Actually, since at least one internal coordinate needs to be used, the method outlined in reference 11 for searching only one semi-infinite strand for localized modes would be an approximation. Except for the local breathing modes, we content

ourselves with saying that a given local mode belongs to one semi-infinite strand or the other, in view of the fact that if one "end" exists in nature then so does the other.

The gap extending from 67.19 to 68.52 cm^{-1} has localized modes at 67.26, 68.10, and 68.37 cm^{-1}. The gap extending from 102.14 to 103.55 cm^{-1} has local modes at 102.50 and 103.54 cm^{-1}. The gap extending from 108.26 to 108.90 cm^{-1} has local modes at 108.46 and 108.74 cm^{-1}. None of the seven localized modes thus far mentioned are hydrogen bond breathing modes.

The gap from 70.38 to 77.58 cm^{-1} is situated between two infinite chain breathing mode branches. We have calculated det$(1 - gC)$ vs. frequency for this gap. The determinant vanishes at 71.35, 73.91, and 76.43 cm^{-1}. The mode at 73.91 cm^{-1} is a localized breathing mode of cell (0), see Fig. 1, which presumably dropped out of the breathing branch directly above. At 400 K it contributes $(0.1\ Å)^2$ to $M^2(0)$. The effect of this mode is essentially gone by the second unit from the cut end, falling off much more rapidly than the perturbed "in band" modes or the "virtual" localized modes.

We have also calculated det$(1 - gC)$ vs. frequency for the gap from 83.72 to 87.69 cm^{-1}. Two local modes appear at 85.49 and 87.06 cm^{-1}. The mode at 85.49 cm^{-1} is a localized breathing mode of cell (-1), see Fig. 1, contributing $(0.12\ Å)^2$ to $\langle M^2(-1)\rangle$ at 400 K. This mode rose out of the breathing branch immediately below.

The average hydrogen bond length is ~2.9 Å. An additional thermal displacement of <0.29 Å would be expected to significantly increase the likelihood of bond dissociation. By considering only the three breathing mode branches and the localized breathing mode, we get (at 400 K) a contribution of $(0.116\ Å)^2$ to $\langle M^2(0)\rangle$ as opposed to $(0.082\ Å)^2$ for $\langle M^2(\infty)\rangle$. We suggest that the enhanced thermal breathing at the terminus should affect the bond-strength parameter for the terminal base pair. The extent of the local mode into the helix, i.e., approximately five base pairs, should give a model for altering Ising model parameters for the five base pairs from the terminus. We suggest that if a free end is available, then a DNA homopolymer may tend to melt first from the ends. An Ising model calculation by Crothers (9) suggests that the effect of the terminus is of only secondary importance in determining the regions most likely to melt. He shows that these regions are primarily determined by the local base-pair sequences, e.g. $\mathcal{AT}$ pairs are less stable than $\mathcal{GC}$ pairs.

An infinite chain "rocking" mode branch extends from 123.89 cm^{-1} at the zone center to 127.99 cm^{-1} at the zone edge, with a minimum of 120.48 cm^{-1} at $\theta \approx 72°$ (7). See Fig. 2 *A*. In a rocking mode the two "outer" hydrogen bond stretches, see Fig. 1, are large but out of phase. The stretching of the "center" bond is about an order of magnitude smaller than either of the other two stretches. Here Im(G) is continuous from 120.48 to 123.89 cm^{-1} and from 123.89 to 127.99 cm^{-1}. Of particular interest is the second region from 124 to 127.5 cm^{-1} as displayed in Fig. 4. Between ~124.75 and ~125.5 cm^{-1} Im$[G(0)]$ is $>(0.01\ Å)^2$ and approaches $(0.02\ Å)^2$ per unit frequency at 300 K typical of the breathing mode displacements described previously. The occurrence of such a rocking mode turning into a breathing mode close to a terminus suggests the possibility that the same phenomenon might occur near other specific sequences of base pairs.

Also of great interest is the resonant behavior of $M^2(0)$ in the low microwave region. The first peak of the lowest acoustic branch occurs at ~1.75 cm^{-1}, thus Im(G) is continuous from 0 to ~1.75 cm^{-1}. See Fig. 5. In Figs. 6–9 we display Im(G) vs. frequency from 0.01 cm to 1.75

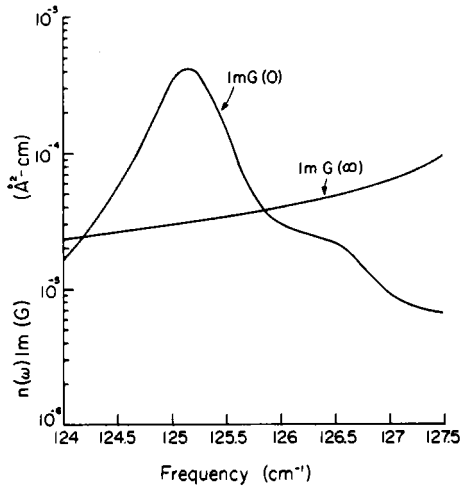

FIGURE 4 Im$G(0)$ and Im$G(\infty)$ for the rocking branch region of 124 to 127.5 cm^{-1}. In the region between 124.5 and 125.5 cm^{-1} the infinite chain rocking modes become terminal breathing modes.

cm^{-1}. Note that the horizontal frequency scales on the four graphs differ. The "upper" curve is Im$[G(0)]$, i.e. proportional to $\rho M^2(0)$. The next two highest curves are Im$G(1)$ and Im$G(3)$ respectively while the "lowest" curve is Im$G(\infty)$, equal to the imaginary part of the perfect helix Green function.

First we will make some general observations regarding this frequency region. The imaginary part of $G(\infty)$ tends to remain at a fairly constant 3×10^{-6} Å^2 per unit frequency interval, $\nu, \nu + \Delta\nu$ (cm^{-1}), $T = 300$ K, except close to the band edges near 0.01 and 1.75 cm^{-1}

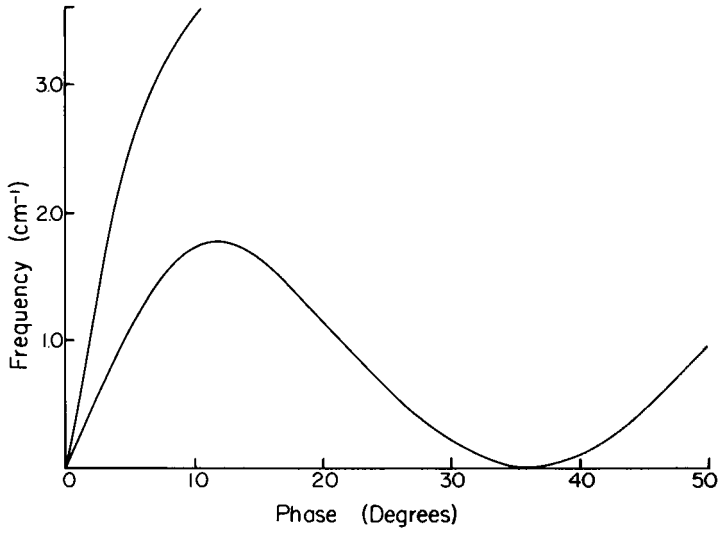

FIGURE 5 The four acoustic mode phonon dispersion branches (2 at $\theta = 0°$, 2 at $\theta = 36°$) for the perfect infinite helix B poly(d$\mathcal{G}$)·poly(d$\mathcal{C}$), up to ~3.5 cm^{-1}. The abscissa is the phase difference between adjacent unit cells. Reproduced with permission from reference 7.

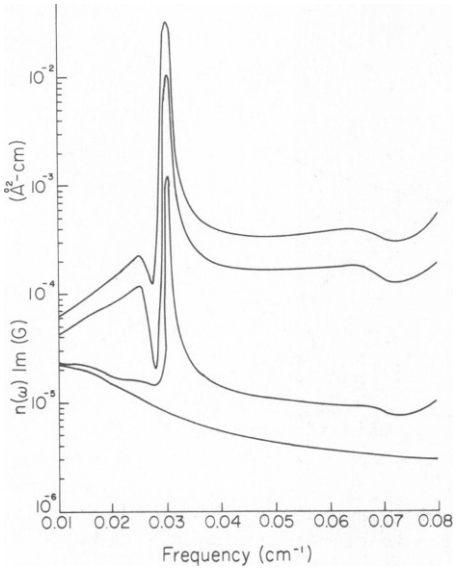

FIGURE 6

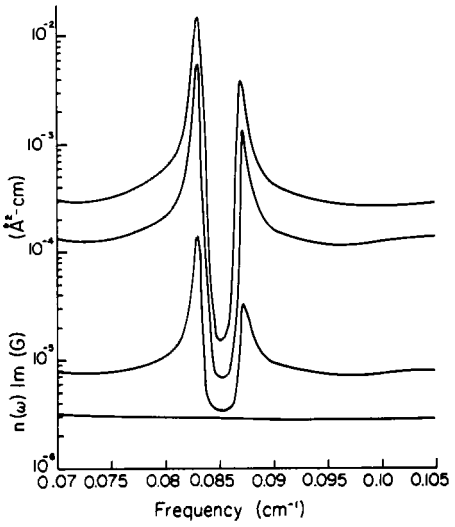

FIGURE 7

FIGURE 6 ImG vs. frequency for the low-microwave region 0.01 cm^{-1} to 0.08 cm^{-1}. The four curves starting from the "lowest" are Im$G(\infty)$, Im$G(3)$, Im$G(1)$ and Im$G(0)$. A pronounced narrow resonant breathing mode of $M(0)$ occurs at 0.03 cm^{-1}.

FIGURE 7 A continuation of Fig. 6 from 0.07 to 0.105 cm^{-1}. Two pronounced narrow resonant breathing modes of $M(0)$ occur at 0.083 and 0.087 cm^{-1}.

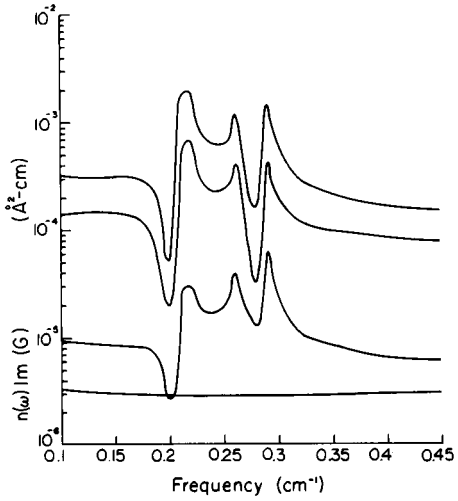

FIGURE 8

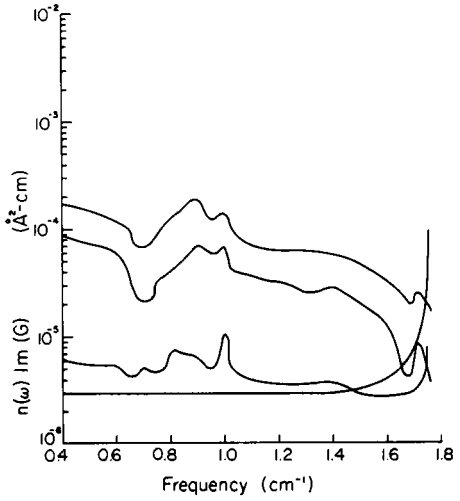

FIGURE 9

FIGURE 8 A continuation of Fig. 7 from 0.1 to 0.45 cm^{-1}. Three broad resonant breathing modes of $M(0)$ occur at 0.22, 0.26, and 0.29 cm^{-1}.

FIGURE 9 A continuation of Fig. 8 from 0.4 to 1.75 cm^{-1} at the first peak in the lowest acoustic branch, see Fig. 5. Resonances with perceptible peaks in $M(0)$ occur at 0.89, 1.0, and 1.7 cm^{-1}.

where $\mathrm{Im}G(\infty)$ increases due to the density of states factor. There are four acoustic mode branches in this frequency region, two at $\theta = 0$ and two at $\theta = 36°$. See Fig. 5. Thus the Green function has four singularities for every frequency in this region. The acoustic modes are discussed in detail in Reference 7. The behavior of $\mathrm{Im}G(0)$ and $\mathrm{Im}G(1)$ is reminiscent of the antinode at the free end of a vibrating chain. The absence of one of the semi-infinite strands has a destabilizing effect resulting in increased amplitude of the hydrogen bond stretching close to the cut end. $\mathrm{Im}G(0)$ and $\mathrm{Im}G(1)$ tend to be in the neighborhood of 10^{-4} Å^2 per unit frequency, with $\mathrm{Im}G(0) \approx 2\ \mathrm{Im}G(1)$, except near the resonances where $\mathrm{Im}G(0)$ can approach 3×10^{-2} Å^2-cm. $\mathrm{Im}G(3)$ is also plotted showing a dramatic fall off in the breathing relative to $M^2(0)$ and $M^2(1)$. Except in the vicinity of the resonances, the effect of the end on the melting coordinate is very small by the sixth unit from the cut, i.e., $\mathrm{Im}G(5) \approx \mathrm{Im}G(\infty)$. At 400 K, the curve $\mathrm{Im}G(0)$ contributes $\approx$ (0.02 Å)^2 to $\langle M^2(0) \rangle$ as opposed to (0.002 Å)^2 for $\langle M^2(\infty) \rangle$ far from the cut.

The features of great interest in these graphs however, are the appearance of narrow resonant melting modes. A resonant melting mode is defined as one where $\mathrm{Re}[\det(1 - gC)] = 0$ and the M^2 amplitude is large. Between 0.01 and 1.75 cm^{-1} the total system of both semi-infinite DNA has 16 resonance modes, at 0.025, 0.03, 0.083, 0.087, 0.17, 0.22, 0.26, 0.29, 0.35, 0.66, 0.72, 0.89, 1.0, 1.6, 1.7 and 1.705 (all in cm^{-1}). The appearance of such resonances is in accordance with the well known fact that a perturbation involving a strong weakening of force constants will produce low lying resonances (16). Presumably, these resonances are approximately evenly divided between the two strands above and below the dashed line in Fig. 1. Again, not unexpectedly, nine of these resonances have perceptible peaks in the $M^2(0)$ coordinate, 0.03, 0.083, 0.087, 0.22, 0.26, 0.29, 0.89, 1.0 and 1.7 cm^{-1}, although only the six modes at 0.03, 0.083, 0.087, 0.22, 0.26, and 0.29 cm^{-1} are clearly $M^2(0)$ resonances.

Below 0.1 cm^{-1} there are three resonances with large amplitude in $M^2(0)$, at 0.03 cm^{-1}, 0.083 cm^{-1} and 0.087 cm^{-1} (~0.9 and 2.5 GHz). In order that these truly be resonances, it must be true that their widths, Γ, be $\ll W$ where W is the width of the band in which they lie. The half-width Γ may be calculated from

$$\Gamma = \frac{2\mathrm{Im}[\det(1 - gC)]}{\mathrm{d}\{\mathrm{Re}[\det(1 - gC)]\}/\mathrm{d}\omega}$$

or may simply be estimated from the graph. The widths of these three resonances are of the order 2.5×10^{-3} cm^{-1}, quite small compared with the band width $W \sim 1.75$ cm^{-1}. Fig. 7 shows how the two resonances near 0.083 and 0.087 "steal" oscillator strength from the modes in the vicinity of 0.085 cm^{-1}. As expected the "higher" frequency resonances tend to be somewhat broader, on the order of 2.5×10^{-2} cm^{-1}.

Two points should be brought to the reader's attention concerning the calculated widths of the low frequency resonances. First, this analysis is in the harmonic approximation. Anharmonic effects will broaden these resonances although it is difficult to estimate to what extent because good estimates for anharmonic force constants are not available and the force field involved is complicated. Second, the effects of damping due to the liquid water environment in which the DNA would find itself in the living cell have not been addressed. These low frequency modes are likely to be highly damped and the resonances broader than our

harmonic calculation would suggest. The quantitative effects of damping on these modes are difficult to ascertain, at present. As a further complication, the degree of damping is expected to depend on the spatial localization of these free end resonances. The qualitative effect will be to broaden the resonances. Energy pumped into these modes will be more readily dispersed into heating of nearby modes and will be less effective in exciting the resonance and its attendent large melting coordinate.

A brief word should be said concerning the positions of the resonances. The accuracy with which the results are reported is meant to distinguish between resonances which are close together, (e.g. 0.083 and 0.087 cm^{-1}), and is not meant to suggest that the positions of the resonances are known to hundreths of a wavenumber. The important point is the prediction that a number of such low frequency resonances exist although their positions are as yet only approximately known.

It is possible that some of the low frequency modes of the DNA helix are over-damped (17), although results (18) from Brillouin scattering measurements on wet DNA fibers and films suggest that at least as low as 5 GHz (about 0.17 cm^{-1}) the modes are not over-damped. In view of the present lack of knowledge concerning the oscillator strengths and widths of these modes, it is difficult to say how significant biologically these low microwave resonances will prove to be. The results of the calculation reported here suggest experiments in which DNA end effects might be observed. For example, the localized breathing modes might be observed in infrared or Raman investigations on solutions containing a large number of short DNA segments. Future experimental work could involve scanning the low microwave region in a search for resonant modes which may manifest themselves as frequencies of enhanced microwave absorption.

APPENDIX A

Evaluation of the Green Function

The Green function $g(\omega^2)$ will be denoted as

$$g(\omega^2) = \int_0^\pi \frac{Q(\theta)\mathrm{d}\theta}{\omega^2 - \omega^2(\theta)}. \tag{A1}$$

The integrand may be singular at one or more points $\omega^2 = \omega^2(\theta_0)$. The singularity is handled by giving ω a small imaginary part (i/τ) and taking the limit as the relaxation time $\tau \to \infty$ (12). Eq. A1 may be rewritten as,

$$g(\omega^2) = \int_0^\pi \left[\frac{Q(\theta)}{\omega^2 - \omega^2(\theta) + i\gamma} - \frac{Q(\theta_0)}{\{[\mathrm{d}\omega^2(\theta_0)]/\mathrm{d}\theta\}(\theta_0 - \theta) + i\gamma}\right]\mathrm{d}\theta + \int_0^\pi \frac{Q(\theta_0)\,\mathrm{d}\theta}{\{[\mathrm{d}\omega^2(\theta_0)]/\mathrm{d}\theta\}(\theta_0 - \theta) + i\gamma} \tag{A2}$$

where the limit $\gamma \to 0$ is understood. The first integral is no longer singular. We may set $\gamma = 0$ and evaluate the integral numerically. The second integral may be handled by use of the identity (12),

$$\lim_{\gamma \to 0^+}\left[\frac{1}{x + i\gamma}\right] = P\left(\frac{1}{x}\right) - i\pi\delta(x)$$

where P denotes the principal part. It is a simple exercise (11) to show that the second integral may be written

$$\left\{\frac{Q(\theta_0)}{[d\omega^2(\theta_0)]/d\theta}\right\}\left\{\log\frac{\theta_0}{\pi-\theta_0}-i\pi\,\mathrm{sgn}\left[\frac{d\omega^2(\theta_0)}{d\theta}\right]\right\}.$$

Note that some care must be taken in the immediate vicinity of the band edges where the slopes of the dispersion curves approach zero. There may be points θ close to the singularity θ_0 such that the condition

$$\frac{1}{2}\left|\frac{d^2\omega^2(\theta_0)}{d\theta^2}(\theta-\theta_0)^2\right| \ll \left|\frac{d\omega^2(\theta_0)}{d\theta}(\theta-\theta_0)\right|$$

is not satisfied. Then the second term in brackets of Eq. A2 will not be a good approximation to the first term for small values of $(\theta-\theta_0)$. Here we may incorporate a finite relaxation time using the scattering formalism described earlier.

The unperturbed solutions, $Q(\theta)$ and $\omega^2(\theta)$, were numerically calculated (7) for 30 values of θ (from 0 to π). We found that the use of the trapezoid rule over these 30 points was sufficient to ensure accurate results as far as 10 units distant from the cut. In the event of a singularity $\omega^2=\omega^2(\theta_0)$, θ_0 and $Q(\theta_0)$ were evaluated using linear interpolation (11). The slope $d\omega^2(\theta_0)/d\theta$ was calculated by placing a second degree polynomial through three neighboring points.

The Green function contains a sum over 123 bands. The "high" frequency bands from 41 to 123 are essentially dispersionless (7), thus we assumed $\omega_\ell^2(\theta)=\omega_\ell^2(0)$ and $q^\ell(\theta)=q^\ell(0)$ for $\ell>40$. The integrations for these bands could then be performed analytically.

APPENDIX B

Defect Problems in Internal Coordinates

Frequently the desired result of a Green's function calculation is to have the values of the displacements for certain internal coordinates while the larger number of Cartesian coordinates determining those internal coordinates may not concern us.

First, note that the mass-weighted Cartesian force constant matrix (F) for the infinite perfect helix may be expressed (19) in terms of the internal force constants (f) as,

$$F_{ij}=\sum_{tt'}B_{ti}f_{tt'}B_{t'j}.$$

Here, B is the transformation from mass-weighted Cartesian coordinates q to internal coordinates S.

Consider the eigenvalue equation to be solved,

$$\sum_j(F_{ij}-\omega^2\delta_{ij}+C_{ij})q_j=0 \tag{B1}$$

where $C_{ij}=-\Sigma_{tt'}B_{ti}^{*}f_{tt'}B_{t'j}$ while the $f_{tt'}$ are the internal force constants connecting unit (-1) to unit (0). For clarity we suppress the double indices previously used. The unit cell and coordinate number (ℓ,α) will be replaced by a single index, say (i), while the Brillouin zone point and branch indices (θ,j) will be denoted as (ℓ). Thus the Green's function for the perfect helix $g=(\omega^2-F)^{-1}$ will be written

$$g_{ij}(\omega^2)=\sum_{\ell}\frac{q_i^{\ell}q_j^{\ell *}}{\Delta_{\ell}}$$

where

$$\Delta_\varrho = \omega^2 - \omega_\varrho^2.$$

Multiplying Eq. B1 on the left by $g = (\omega^2 - F)^{-1}$ yields

$$q_i + \sum_{\substack{\varrho,t,t' \\ k,j}} \left[\frac{q_i^\varrho q_k^{\varrho^*}}{\Delta_\varrho} B_{tk}^* f_{tt'} B_{t'j} q_j \right] = (q_0)_i \tag{B2}$$

or

$$q_i + \sum_{\varrho,t,t'} \left(\frac{q_i^\varrho S_t^{\varrho^*}}{\Delta_\varrho} \right) f_{tt'} S_{t'} = (q_0)_i \tag{B3}$$

where we have used the transformation property

$$S_t = \sum_i B_{ti} q_i. \tag{B4}$$

Multiplying Eq. B3 by $B_{t''i}$ and summing over i while using Eq. B4 yields

$$S_{t''} + g_{t''t} f_{tt'} S_{t'} = (S_0)_{t''} \tag{B5}$$

where the perfect helix internal coordinate Green function

$$g_{tt'} = \sum_\varrho \frac{S_t^\varrho S_{t'}^{\varrho^*}}{\Delta_\varrho}.$$

Note that if Eq. B2 is satisfied, then Eq. B5 will be satisfied, although the existence of a solution in internal coordinates does not guarantee the existence of one in Cartesian coordinates. This is simply a result of the fact that the transformation B does not have an inverse due to the possible redundancy of the internal coordinates S. This does not present a problem for frequencies lying within one or more dispersion branches since in those regions, Eq. B2 always has a solution as therefore does Eq. B5. In the process of searching for local modes within the band gaps, however, one must be careful to check that $|1 - g(\omega^2)C| = 0$ in Cartesian coordinates for each ω^2 that yields $|1 + g(\omega^2)f| = 0$ in internal coordinates.

It remains to be shown that the quantity $[(1 + gf)^{-1}g]_{tt'}$ is equivalent to the severed helix internal coordinate Green function

$$G_{tt'}(\omega^2) = \sum_{\omega'} \frac{S_t(\omega') S_{t'}^*(\omega')}{\Delta(\omega')}$$

where the $S_t(\omega)$ are the perturbed normal mode internal coordinates. Had a driving force (E_i) been added to the right side of Eq. B1, then Eq. B5 (with the incoming wave S_0 set to zero) would have yielded for the driven $\mathcal{S}$:

$$\mathcal{S}_t = - \sum_{t',i} (1 + gf)_{tt'}^{-1} g_{t'i} E_i$$

where

$$g_{ti} = \sum_\varrho \frac{S_t^\varrho q_i^{\varrho^*}}{\Delta_\varrho}.$$

However $\mathcal{S}_t = -\Sigma_i G_{ti} E_i$ by definition of G. Thus

$$\sum_{i''} (1 + gf)^{-1}_{ti''} g_{i''i} = G_{ti} = \sum_{\omega'} \frac{S_t(\omega') q_i^*(\omega')}{\Delta(\omega')} \tag{B6}$$

where the $q_i(\omega)$ are the perturbed normal mode Cartesian coordinates. Finally, postmultiplication of Eq. B6 by $B^*_{i'i}$ and summation over i yields:

$$[(1 + gf)^{-1} g]_{ti'} = \sum_{\omega'} \frac{S_t(\omega') S_{i'}^*(\omega')}{\Delta(\omega')} .$$

APPENDIX C

The Chain-severing Perturbation

The helix has been severed at the points where the restriction endonuclease enzymes (20) cleave the DNA, see Fig. 1. The valence coordinates directly affected by the cut and the associated force constant are listed in Table I.

A long range (over one helical turn) Coulomb interaction has been built into the perfect helix calculation (7). The strength of the interaction was chosen so as to reproduce an experimental value (18) for the longitudinal sound velocity. Due to this interaction, the number of coordinates directly affected by the cut is too large to manage. This problem was overcome by projecting out appropriate internal coordinates and matching the resulting new potential energy to that used in the perfect helix calculation.

The interaction between the two units immediately adjacent to the cut turns out to be more than an order of magnitude larger than say, the interaction between units (-1) and (1). Between the two cells (-1) and (0), there are four pairs of intercell bases, $\mathcal{G}^{-1}\mathcal{G}^0$, $\mathcal{C}^{-1}\mathcal{C}^0$, $\mathcal{G}^{-1}\mathcal{C}^0$ and $\mathcal{C}^{-1}\mathcal{G}^0$. For each of these four pairs of bases we constructed (11) a compression, shearing and tilting coordinate, and matched the resulting potential to the potential used in the unperturbed calculation (11).[1] The calculated force constants are listed in Table I. We note that the calculated torsion potential resulting from the interbase shearing is in excellent agreement[1] with a value reported by Barkley and Zimm (17).

Finally we need to take into account the longer range interaction between the units not including the two units adjacent to the cut. As the distance (r) between the unit cells considered increases, the compressional interaction falls off like $1/r^3$ whereas the shearing potential falls off like $1/r^5$, see reference 11 and footnote 1. The major effect of this long-range interaction is a compressional force.

A generalized compression coordinate is constructed as,

$$S = \sum_{\ell,r} \frac{(\Delta S_z)_{\ell,r}}{R^{3/2}_{\ell,r}} . \tag{C1}$$

Here ℓ refers to a unit cell on the "left" side of the cut and r refers to a cell on the "right" side of the cut ≤ 9 base-pair units distant from ℓ. $(\Delta S_z)_{\ell,r}$ is the relative z displacement of the centers of mass of base pairs $(\mathcal{GC})_r$ and $(\mathcal{GC})_\ell$ while the weighting factor $R_{\ell,r}$ is the distance between the respective centers of mass. The force constant was chosen so as to match the perfect helix long-wavelength compression potential (11).[1]

For frequencies $> \approx 20$ cm^{-1} it was not necessary to separately consider the two units adjacent to the cut. The long-range interaction was taken into account by a generalized compression coordinate, Eq. C1, where the term $\ell = -1, r = 0$ was included in the sum.

---

[1]Putnam, B. F., E. W. Prohofsky, and L. L. Van Zandt. Calculated compression, bending, shearing, torsion, and base tilting force constants of B and A poly(d$\mathcal{G}$) · poly(d$\mathcal{C}$). Submitted for publication.

TABLE I

INTERNAL COORDINATE FORCE CONSTANTS AFFECTED BY CUT

Internal coordinate*	Type	Force constant‡
$P9^{-1}(\mathcal{G}) - 01^{\circ}(\mathcal{G})$	stretch	3.451
$P9^{-1}(\mathcal{G}) - 01^{\circ}(\mathcal{G}) - C3^{\circ}(\mathcal{G})$	angle bend	0.772
$01^{\circ}(\mathcal{G})$—$P9^{-1}(\mathcal{G})$—$04^{-1}(\mathcal{G})$	angle bend	0.620
$01^{\circ}(\mathcal{G})$—$P9^{-1}(\mathcal{G})$—$02^{-1}(\mathcal{G})$	angle bend	0.670
$01^{\circ}(\mathcal{G})$—$P9^{-1}(\mathcal{G})$—$03^{-1}(\mathcal{G})$	angle bend	0.670
$P9^{-1}(\mathcal{G})$—$C3^{\circ}(\mathcal{G})$	nonbonded stretch	0.150
$01^{\circ}(\mathcal{G})$—$04^{-1}(\mathcal{G})$	nonbonded stretch	0.170
$01^{\circ}(\mathcal{G})$—$02^{-1}(\mathcal{G})$	nonbonded stretch	0.397
$01^{\circ}(\mathcal{G})$—$03^{-1}(\mathcal{G})$	nonbonded stretch	0.397
$P9^{\circ}(\mathcal{C})$—$01^{-1}(\mathcal{C})$	stretch	3.451
$P9^{\circ}(\mathcal{C})$—$01^{-1}(\mathcal{C})$—$C3^{-1}(\mathcal{C})$	angle bend	0.772
$01^{-1}(\mathcal{C})$—$P9^{\circ}(\mathcal{C})$—$04^{\circ}(\mathcal{C})$	angle bend	0.620
$01^{-1}(\mathcal{C})$—$P9^{\circ}(\mathcal{C})$—$02^{\circ}(\mathcal{C})$	angle bend	0.670
$01^{-1}(\mathcal{C})$—$P9^{\circ}(\mathcal{C})$—$03^{\circ}(\mathcal{C})$	angle bend	0.670
$P9^{\circ}(\mathcal{C})$—$C3^{-1}(\mathcal{C})$	nonbonded stretch	0.150
$01^{-1}(\mathcal{C})$—$04^{\circ}(\mathcal{C})$	nonbonded stretch	0.170
$01^{-1}(\mathcal{C})$—$02^{\circ}(\mathcal{C})$	nonbonded stretch	0.397
$01^{-1}(\mathcal{C})$—$03^{\circ}(\mathcal{C})$	nonbonded stretch	0.397
$P9^{-1}(\mathcal{G})$—$01^{\circ}(\mathcal{G})$	torsion	0.023
$P9^{\circ}(\mathcal{C})$—$01^{-1}(\mathcal{C})$	torsion	0.023
$\mathcal{G}^{-1}, \mathcal{G}^{\circ}$	compression§	0.0289
$\mathcal{C}^{-1}, \mathcal{C}^{\circ}$	compression	0.0160
$\mathcal{G}^{-1}, \mathcal{C}^{\circ}$	compression	0.0054
$\mathcal{C}^{-1}, \mathcal{G}^{\circ}$	compression	0.0035
$\mathcal{G}^{-1}, \mathcal{G}^{\circ}$	shearing§	0.0068
$\mathcal{C}^{-1}, \mathcal{C}^{\circ}$	shearing	0.0043
$\mathcal{G}^{-1}, \mathcal{C}^{\circ}$	shearing	0.0068
$\mathcal{C}^{-1}, \mathcal{G}^{\circ}$	shearing	0.0043
$\mathcal{G}^{-1}, \mathcal{G}^{\circ}$	tilting§	0.0555
$\mathcal{C}^{-1}, \mathcal{C}^{\circ}$	tilting	0.0237
$\mathcal{G}^{-1}, \mathcal{C}^{\circ}$	tilting	0.0118
$\mathcal{C}^{-1}, \mathcal{G}^{\circ}$	tilting	0.0067
$(\mathcal{GC})_{\ell}, (\mathcal{GC})_{r}$	generalized compression§‖	0.1861¶
$(\mathcal{GC})_{\ell}, (\mathcal{GC})_{r}$	generalized compression§**	0.1729

*The superscript indicates the unit cell number while ($\mathcal{G}$) or ($\mathcal{C}$) denote the guanine or cytosine strand, respectively.

‡Force constants are in mdyne/Å or mdyne-Å/rad^2 as appropriate.

§See section discussing the breaking of the long-range electrostatic interaction.

‖The term ($\ell = -1, r = 0$) not in potential sum for matching.

¶The generalized compression force constants have units mdyne-Å^2 due to a weighting factor $R^{-3/2}$ in the internal coordinate.

**The term ($\ell = -1, r = 0$) included in potential sum for matching.

As a final approximation, we mention that the weak single bond torsional forces about the backbone adjacent to those two bonds directly severed, were not taken into account. In some preliminary calculations however, we did include them in the perturbation and found that essentially the same results would be obtained (for the frequencies scanned in this work) if these weak forces were ignored. The single bond torsions about the two bonds directly severed were included in the perturbation.

This work was supported in part by National Science Foundation grant DMR 78-20602 and National Institutes of Health grant GM24443.

Received for publication 12 September 1980 and in revised form 2 March 1981.

REFERENCES

1. Eyster, J. M., and E. W. Prohofsky. 1977. On the B to A conformation change of the double helix. *Biopolymers.* 16:965–982.
2. Prohofsky, E. W., K. C. Lu, L. L. Van Zandt, and B. F. Putnam. 1979. Breathing modes and induced resonant melting of the double helix. *Phys. Lett.* 70A:492–494.
3. Higgs, P. W. 1953. The vibration spectra of helical molecules: infra-red and Raman selection rules, intensities and approximate frequencies. *Proc. R. Soc. Lond. A.*220:472–485.
4. Lifshitz, I. M., and S. I. Pekar. 1955. Tamm connected states of electrons on the surface of a crystal and the surface oscillations of the atoms of a lattice. *Uspekhi Fiz. Nauk.* 56:531–568.
5. Crothers, D. M. 1968. Calculation of melting curves for DNA. *Biopolymers.* 6:1391–1404.
6. Azbel, M. Ya. 1979. Phase transitions in DNA. *Phys. Rev. A.* 20:1671–1684.
7. Mei, W. N., M. Kohli, E. W. Prohofsky, and L. L. Van Zandt. 1981. Acoustic modes and nonbonded interactions of the double helix. *Biopolymers.* 20:833–852.
8. Grundler, W., and F. Keilman. 1978. Nonthermal effects of millimeter microwaves on yeast growth. *Z. Naturforsch.* 33C:15–18.
9. Kohli, M., W. N. Mei, E. W. Prohofsky, and L. L. Van Zandt. 1981. Calculated microwave absorption of double helical B poly(dG)·poly(dC). *Biopolymers.* 20:853–864.
10. Swicord, M. L. 1980. Studies of Microwave Absorption in Liquids by Optical Heterodyne Detection of Thermally Induced Refractive Index Fluctuations. Thesis, University of Maryland, College Park, Maryland. Chap. 5.
11. Putnam, B. F. 1981. Calculation of Macromolecular Force Constants and Vibrational Properties of a Semi-Infinite Strand of the DNA Double Helix. Ph.D. Thesis, Purdue University, West Lafayette, Indiana. Chap. 4.
12. Elliott, R. J. 1975. Proceedings of the International School of Physics, Course LV, Lattice Dynamics and Intermolecular Forces. Academic Press Inc., New York. 342–383.
13. Callaway, J. 1974. Quantum Theory of the Solid State, A and B. Academic Press Inc., New York. 824 pp.
14. Maradudin, A. A., E. W. Montroll, G. H. Weiss, and I. P. Ipatova. 1971. Theory of Lattice Dynamics in the Harmonic Approximation. Academic Press, Inc., New York. 353–519.
15. Conte, S. D., and C. de Boor. 1972. Elementary Numerical Analysis. McGraw Hill Publications, New York. 31–32.
16. Page, J. B., Jr. 1974. Defect-induced resonance modes in the asymptotic limit of low frequencies: isotope effects and amplitude patterns. *Phys. Rev. B* 10:719–738.
17. Barkley, M. D., and B. H. Zimm. 1979. Theory of twisting and bending of chain macromolecules; analysis of the fluorescence depolarization of DNA. *J. Chem. Phys.* 70:2991–3007.
18. Maret, G., R. Oldenbourg, G. Winterling, K. Dransfeld, and A. Rupprecht, 1979. Velocity of high frequency sound waves in oriented DNA fibres and films determined by Brillouin scattering. Colloid Polym. Sci. 275:1017–1020.
19. Steele, D. 1971. Theory of Vibrational Spectroscopy. W. B. Saunders Co., Philadelphia 18–37.
20. Lewin, B. 1974. Gene Expression. Vol. 1. John Wiley & Sons, New York. 490–492.